A Simulation Study of the Effect of Ionospheric Vertical Gradients on the Neutral Bending Angle Error for GNSS Radio Occultation

V. L. Barbosa[1], **J. Rasch**[2], **A. Carlström**[3], **M. I. Pettersson**[1], **and V. T. Vu**[1]

[1]Blekinge Institute of Technology, Sweden
[2]Molflow, Sweden
[3]RUAG Space AB, Sweden

Abstract— Radio Occultation based on Global Navigation Satellite System signals (GNSS RO) is an increasingly important remote sensing technique. Its measurements are used to derive parameter of the Earth's atmosphere, e.g., pressure, temperature and humidity, with good accuracy. The systematic residual error present on the data processing is related to ionospheric conditions, such as the distribution of electrons and the resultant vertical gradient. This study investigates the relationship between these parameters and the residual ionospheric error (RIE) on the retrieved bending angle in the stratosphere. Chapman function combined to sinusoidal perturbations are used to model electron density profiles and compared to RO retrievals of the ionosphere to perform the investigation. The results confirmed that the major ionospheric influence on the retrieval error is related to the F-layer electron density peak, whereas small-scale vertical structures play a minor role.

1. INTRODUCTION

Radio Occultation (RO) is a remote sensing technique, firstly applied to investigate planetary atmospheres in the Solar System. RO became a feasible source of measurements of the Earth's atmosphere since the Global Positioning System (GPS) turned into a reliable service in the 90's [1]. The technique relies on Global Navigation Satellite Systems (GNSS) signals intercepted by a Low-Earth Orbit (LEO) satellite. The fundamental signal measurement on the LEO satellite is the Doppler shift, which allows the derivation of the very basic product of the GNSS RO. The retrieved bending angle (α) is a record of the atmospheric characteristics. It describes the effect of refraction throughout the propagation of the signal between the GNSS and LEO satellites. The dynamics of the transmitter and receiver yields a scanning motion from the upper atmosphere (LEO orbit) down to the Earth limb.

Consequently, the scanning capability of different atmospheric layers is related mainly to the orbit of the LEO satellite and the purpose of each radio occultation mission. For instance, the Constellation Observing System for Meteorology Ionosphere and Climate (COSMIC) is composed by LEO satellites orbiting around 700 and 800 km, intended to investigate not exclusively the neutral atmosphere (stratosphere and troposphere) but also the upper atmosphere (ionosphere) [2].

The RO data product has been mostly applied in Numerical Weather Prediction (NWP) [3]. Regarding the weather on Earth, the stratospheric and tropospheric conditions are of major interest, as well as the accuracy of these measurements. However, the bending angle (BA) on the lower-part of the atmosphere holds signatures of the bending added in the ionosphere and therefore may differ for different signal trajectories and different satellite altitudes (i.e., different atmospheric layers included). This fact implies the bending associated to the ionosphere must be removed to such application.

Different methods have been proposed in order to cancel out the ionospheric effect. The dispersion method [4] is the most known and usually named as standard ionospheric correction. Its main advantage is simple implementation and no prior information about the ionospheric conditions required. However, the dispersion method removes only the first order term of the ionospheric contribution. Lately, a modification of the standard correction has been proposed in order to remove the second order term, which is only feasible once the features of the ionosphere are known a priori. The kappa method is aimed to climatology or climate changing monitoring and, therefore, applicable on monthly-average bending angle measurements. It is dependent either on ionospheric measurements [5] or on geophysical parameters such as solar zenith angle, solar flux and altitude [6].

Despite the method chosen to perform the ionospheric correction, small and large-scale structures present on the Ionosphere are related to the residual ionospheric error (RIE). Moreover, it is known that the level of perturbation observed yields different levels of RIE [7–10].

In this paper, small-scale structures are modelled on the ionosphere as sinusoidal perturbations. The vertical gradient and their influence on the RIE after the standard ionospheric correction are evaluated. The analysis also takes into account the influence of the electron density peak on the F-layer range. This paper is divided in six sections. Sections 2 and 3 describe the standard ionospheric correction and how different ionospheric scenarios have been modelled for the present analysis, respectively. Section 4 presents an overview of the selected conditions to be evaluated. Finally, Sections 5 and 6 present the results of the simulations and final remarks.

2. STANDARD IONOSPHERIC CORRECTION

Conventionally, RO data processing is performed on the measurements of GNSS signals in L_1 (1575.42 MHz) and L_2 (1227.60 MHz) bands. According to the dispersion method [4], the corrected bending angle (α_c) can be calculated from the retrieved $\alpha_{L1,L2}$ as a function of a common impact height (a),

$$\alpha_c(a) = \frac{\alpha_{L1}(a)\, {f_{L1}}^2 - \alpha_{L2}(a)\, {f_{L2}}^2}{{f_{L1}}^2 - {f_{L2}}^2}. \tag{1}$$

Based on the corrected bending angle, tropospheric parameters such as pressure, temperature and humidity are retrieved. Despite the advantages, i.e., low complexity and no prior knowledge of the ionospheric conditions, the dispersion method relies on the fact GNSS signals are propagated in the same trajectory, regardless of their frequency. In fact, this fundamental condition is not totally satisfied. Ray tracing simulations [11–13] have shown the difference between the ray path of L1 and L2 signals can reach the order of kilometers depending on the distribution of electrons in the ionosphere. As a consequence, the retrieved bending angles do not have the same impact height [14]. Thus, Equation (1) includes an inherent error on the corrected bending angle. The residual ionospheric error is the source of the bias present in any atmospheric parameter derived from the corrected bending angle. For instance, the temperature error derived from RO data can reach approximately 0.3 K at 30 km altitude [15]. The RIE is denoted as

$$\Delta\alpha = \alpha_c - \alpha_n, \tag{2}$$

where α_n stands for the bending angle after propagation in the neutral atmosphere.

3. IONOSPHERIC MODEL

In order to analyse the influence of different ionospheric scenarios on the neutral bending angle error, the ionosphere has been modeled by the asymmetric Chapman layer function [16], which is defined as

$$\begin{aligned} \rho(r) &= \rho_{\max} \exp\left(\frac{1}{2}(1 - u - e^{-u})\right), \\ u &= (r - r_0)/H, \end{aligned} \tag{3}$$

where $\rho_{\max}$ is the F-layer electron density peak at r_0 (km), r is the radius height (km) from the Earth center and H stands for scale height (km).

Equation (3) is used to model E and F-layer separately. Consequently, the electron density profile outcome is defined by two electron density peaks ($\rho_{\max\, E,F}$), heights ($r_{0E,F}$) and scale heights ($H_{E,F}$),

$$\rho_{\,iono}(r) = \rho_E(r) + \rho_F(r), \tag{4}$$

in which ρ_E shapes essentially the distribution of electron within 80 and 150 km and ρ_F from 150 up to 650 km.

Equation (4) can be easily adapted in order to add a perturbation to either E or F term, as an artifact to model vertical gradients along the ionosphere. For the analysis presented in this paper, the sinusoidal perturbation was combined to the F term. Then, Equation (4) is rewritten as

$$\begin{aligned} \rho_{\,iono}(r) &= \rho_E(r) + \delta\, \rho_F(r), \\ \delta &= 1 + \beta \sin(2\pi r/L_0), \end{aligned} \tag{5}$$

where β is the amplitude of the sinusoidal perturbation, given in percentage, and L_0 is the oscillation period (km). The electron density profile is converted to refractivity and combined to the

exponential neutral atmosphere as [17]

$$\begin{aligned} n_{ionoL_1,L_2}(r) &= \frac{40.3\,\rho(r)}{f^2_{L_1,L_2}}, \\ N_{L_1,L_2}(r) &= N_{neutral}(r) - \frac{(n_{ionoL_1,L_2}(r)-1)}{1\cdot 10^{-6}}, \\ N_{neutral}(r) &= N_0 \exp(-r/H_0), \end{aligned} \tag{6}$$

where N_0 is refractivity at the ground (350 km) and H_0 the scale height (8 km) for the refractivity.

4. SIMULATION

The F-layer electron density peak varies during day and night-time, mostly related to low or high solar activity periods. Therefore, the sinusoidal perturbations have been combined to such a range of peak values. Regarding the vertical gradients, cases assuming $\beta = (0, 0.01, 0.03, 0.10)$ have been considered. In this context, case $\beta = 0$ represents a scenario without perturbation, called in this paper as clean. All the cases considering some level of oscillation are referred as disturbed. The oscillation period $L_0 = 5$ km has been assumed for every case. Figure 1(a) depicts the electron density profiles (clean cases) given by Equation (4) and Figure 1(b) presents in detail a profile considering additional wave structures described by Equation (5).

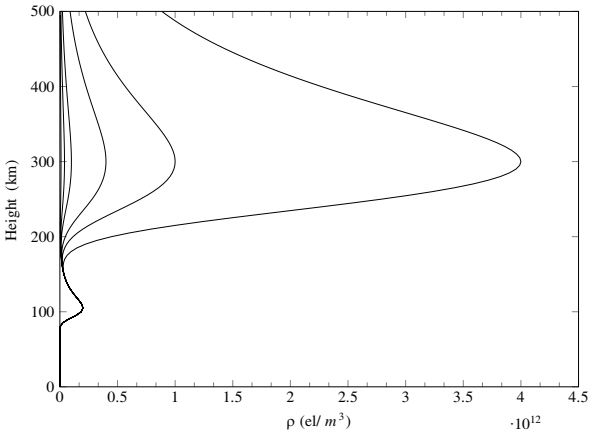

(a) Electron density profiles without perturbation.

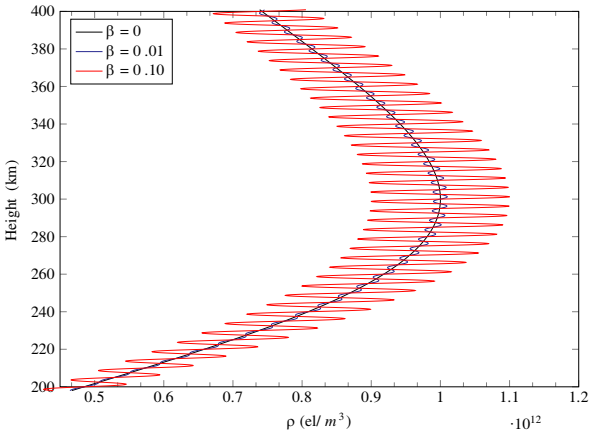

(b) Zoomed region for curve $\rho_F = 1\cdot 10^{12}$ with $\beta = 0$, $\beta = 0.01$ and $\beta = 0.10$.

Figure 1: Electron density profile presented in (a) using $H_E = 10$ km, $H_F = 50$ km, $r_{0E} = 105$ km, $r_{0F} = 300$ km, $\rho_{\max E} = 2\cdot 10^{11}$ and $\rho_{\max F} = (1\cdot 10^{11}, 4\cdot 10^{11}, 1\cdot 10^{12}, 4\cdot 10^{12}, 1\cdot 10^{13})$el/$m^3$.

For comparison with more realistic conditions, some cases have been selected from a dataset of an empirical model for the ionospheric electron density [18]. The dataset gathers ionospheric profiles inverted from raw COSMIC measurements. In [18], the authors also proposed a scintillation index, or Occultation Scintillation Index Proxy (OSPI), as metric to categorize electron density profiles regarding the presence of disturbances. OSPI is defined as the standard deviation normalized by ρ_F of the difference between consecutive samples points on the electron density profile within $r_{\min}$ and $r_{\max}$ height range,

$$OSPI = \frac{\sigma\Delta\rho(r_{\min}, r_{\max})}{\rho_F} \tag{7}$$

For the index calculation, the distance considered between consecutive points was 1 km. The standard deviation was calculated within 550 km ($r_{\min}$) and 650 km ($r_{\max}$). Assuming clean profiles as the ones with $OSPI < 0.001$ and disturbed as $OSPI > 0.031$, 10 clean and 10 disturbed profiles have been selected including the minimum and maximum F-layer electron density peaks profiles observed in the dataset. Figure 2 presents the selected electron density profiles.

A wave optics propagator assuming Multiple Phase Screen technique [19, 20] has been implemented to simulate the propagation of the GNSS signals through the Earth's atmosphere. Our simulations considered exponential neutral refractivity for both analytic and realistic cases. The reference bending angle (α_n), required to performed the standard ionospheric correction and given

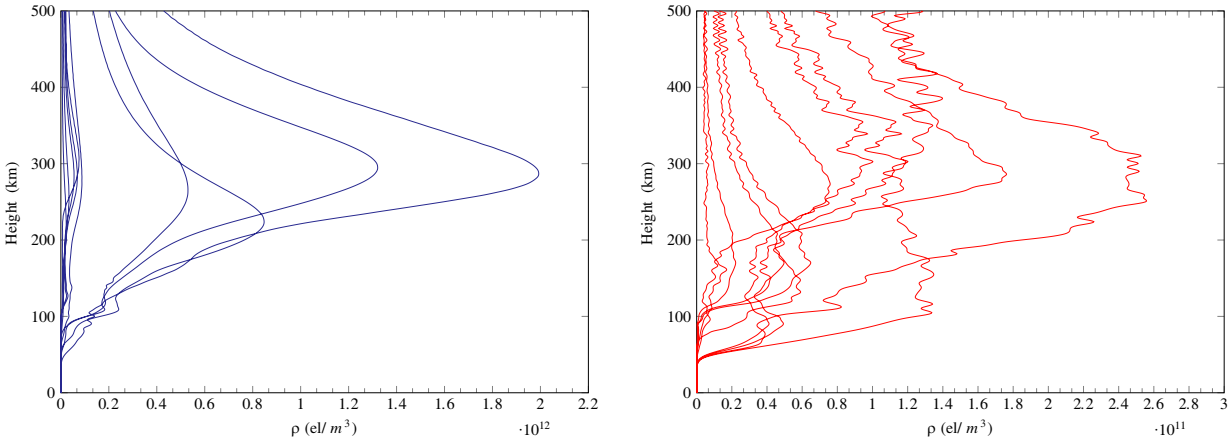

(a) Clean (b) Disturbed

Figure 2: Set of realistic (a) clean and (b) disturbed electron density profiles.

by Equation (1), is retrieved from Abel Transform and assumes an neutral atmosphere with exponential refractivity as well.

5. RESULTS

The neutral bending angle error, the difference between the corrected bending angle (α_c) and the one neglecting ionosphere, have been calculated within the impact height range of 20 km and 40 km. Figure 3 depicts the maximum bending angle error for every simulated scenario as a function of the electron density peak in F-layer.

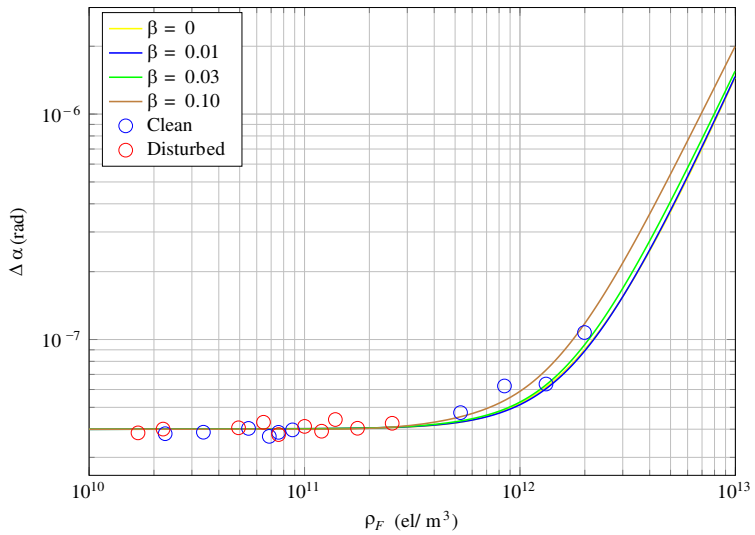

Figure 3: Residual Ionospheric Error comparison between analytic model and realistic cases (Clean and Disturbed).

The dependence of the residual ionospheric error regarding the ionospheric conditions is clearly stressed on the curves. The RIE increases mainly due to the influence of the F-layer electron density peak. The solid curves are roughly equal, which means presence of disturbance on the analytic electron density profiles produced a small contribution on the RIE. The same trend is observed between clean (blue circles) and disturbed (red circles) dataset profiles. Overall, analytic and dataset profiles presented good agreement regarding RIE. A better fitting would be possible if parameters such as scale height ($H_{E,F}$), electron density peaks and height ($\rho_{\max}, r_0$) would be adjusted. Further, RIE for cases with $\rho_F < 2 \cdot 10^{11}$ are mostly limited to the numerical noise floor in our MPS implementation.

6. CONCLUSION

The residual ionospheric error affects significantly the accuracy of radio occultation measurements. This work presented an analysis of the residual ionospheric error on the corrected bending angle in lower altitudes (stratosphere). Parameters such as small-scale vertical structures and F-layer electron density peak had their influence evaluated. The results depict a good agreement between analytic and dataset profiles regarding the RIE. However, this may on the other hand be the result of the limited dataset used on this study. For instance, the maximum F-layer electron density for disturbed cases is not as great as observed in clean cases.

The influence of F-layer electron density peak, and consequently the total electron content (TEC) and the gradient caused by the F-layer bulge, has a major contribution on the RIE, whereas small-scale vertical structures on the electron density profiles presented a minor influence.

Further investigation must be performed in order to fully gauge the effect of electron density perturbations on the RIE assuming a larger statistical survey of measured ionospheric profiles.

REFERENCES

1. Kursinski, E. R., G. A. Hajj, J. T. Schofield, R. P. Linfield, and K. R. Hardy, "Observing Earth's atmosphere with radio occultation measurements using the global positioning system," *Journal of Geophysical Research Atmospheres*, Vol. 102, No. 19, 23429–23465, 1997.
2. Anthes, R. A., P. A. Bernhardt, Y. Chen, L. Cucurull, K. F. Dymond, D. Ector, S. B. Healy, S.-P. Ho, D. C. Hunt, Y.-H. Kuo, H. Liu, K. Manning, C. McCormick, T. K. Meehan, W. J. Randel, C. Rocken, W. S. Schreiner, S. V. Sokolovskiy, S. Syndergaard, D. C. Thompson, K. E. Trenberth, T.-K. Wee, N. L. Yen, and Z. Zeng, "The Cosmic/formosat-3 mission: Early results," *Bulletin of the American Meteorological Society*, Vol. 89, No. 3, 313–333, 2008,
3. Anthes, R. A., C. Rocken, and Y. H. Kuo, "Applications of COSMIC to meteorology and climate," *Terrestrial, Atmospheric and Oceanic Sciences*, Vol. 11, No. 1, 115–156, March 2000.
4. Vorob'ev, V. V. and T. G. Krasil'nikova, "Estimation of the accuracy of the atmospheric refractive index recovery from doppler shift measurements at frequencies used in the NAVSTAR system," *USSR Phys. Atmos. Ocean, Engl. Transl.*, Vol. 29, No. 5, 602–609, 1994.
5. Healy, S. B. and I. D. Culverwell, "A modification to the standard ionospheric correction method used in GPS radio occultation," *Atmospheric Measurement Techniques*, Vol. 8, No. 8, 3385–3393, August 2015, http://www.atmos-meas-tech.net/8/3385/2015/.
6. Angling, M. J., S. Elvidge, and S. B. Healy, "Improved model for correcting the ionospheric impact on bending angle in radio occultation measurements," *Atmospheric Measurement Techniques*, 2017, https://www.atmos-meas-tech-discuss.net/amt-2017-162/amt-2017-162.pdf.
7. Pavelyev, A. G., Y. A. Liou, J. Wickert, T. Schmidt, A. A. Pavelyev, and S. F. Liu, doi10.1029/2006JA011625, "Effects of the ionosphere and solar activity on radio occultation signals: Application to CHAllenging Minisatellite Payload satellite observations," *Journal of Geophysical Research: Space Physics*, Vol. 112, No. 6, 2007.
8. Pavelyev, A., T. Tsuda, K. Igarashi, Y. A. Liou, and K. Hocke, "Wave structures in the electron density profile in the ionospheric D- and E-layers observed by radio holography analysis of the GPS/MET radio occultation data," *Journal of Atmospheric and Solar-Terrestrial Physics*, Vol. 65, No. 1, 59–70, 2003.
9. Matyugov, S. S., O. I. Yakovlev, A. G. Pavelyev, A. A. Pavelyev, and V. A. Anufriev, "Sporadic structures in the equatorial ionosphere from the GPS: Formosat-3 radio-occultation experiments," *Radiophysics and Quantum Electronics*, Vol. 58, No. 4, 233–244, 2015.
10. Igarashi, K., A. Pavelyev, K. Hocke, D. Pavelyev, and J. Wickert, "Observation of wave structures in the upper atmosphere by means of radio holographic analysis of the radio occultation data," *Advances in Space Research*, No. 6-7, 1321–1326, Vol. 27, January 2001, http://linkinghub.elsevier.com/retrieve/pii/S0273117701001442.
11. Hoque, M. M. and N. Jakowski, "Mitigation of higher order ionospheric effects on GNSS users in Europe," *GPS Solutions*, Vol. 12, No. 2, 87–97, 2007, https://link.springer.com/content/pdf/10.1007/s10291-007-0069-5.pdf.
12. Hoque, M. M. and N. Jakowski, "Estimate of higher order ionospheric errors in GNSS positioning," *Radio Science*, Vol. RS5008, 2008
13. Hoque, M. M. and N. Jakowski, "Ionospheric bending correction for GNSS radio occultation signals," *Radio Science*, Vol. 46, No. 6, December 2011, http://doi.wiley.com/10.1029/2010RS004583.

14. Coleman, C. J. and B. Forte, "On the residual ionospheric error in radio occultation measurements," *Radio Science*, June 2017, http://doi.wiley.com/10.1002/2016RS006239.
15. Mannucci, A. J., C. O. Ao, X. Pi, and B. A. Iijima, "The impact of large scale ionospheric structure on radio occultation retrievals," *Atmospheric Measurement Techniques*, Vol. 4, No. 12, 2837–2850, Dec. 2011, http://www.atmos-meas-tech.net/4/2837/2011.
16. Chapman, S., "The absorption and dissociative or ionizing effect of monochromatic radiation in an atmosphere on a rotating earth part II. Grazing incidence," *Proceedings of the Physical Society*, Vol. 43, No. 5, 483, 1931http://stacks.iop.org/0959-5309/43/i=5/a=302.
17. Culverwell, I. D. and S. B. Healy, "Simulation of L1 and L2 bending angles with a model ionosphere," Tech. Rep., Danish Meterological Institute, Copenhagen, 2015.
18. Garcia-Fernandez, M., M. Hernandez-Pajares, A. Rius, R. Notarpietro, A. V. Engeln, and Y. Béniguel, "Empirical model of the ionosphere based on COSMIC/FORMOSAT-3 for neutral atmosphere radio occultation processing," *Atmospheric Measurement Techniques*, 1–13, July 2017.
19. Knepp, D. L., "Multiple phase-screen calculation of the temporal behavior of stochastic waves," *Proceedings of the IEEE*, Vol. 71, No. 6, 722–737, June 1983,
20. Sokolovskiy, S. V., "Modeling and inverting radio occultation signals in the moist troposphere," *Radio Science*, Vol. 36, No. 3, 441–458, May 2001, http://doi.wiley.com/10.1029/1999RS002273.